

# Antimagnetic rotation and sudden change of electric quadrupole transition strength in $^{143}\text{Eu}$

S. Rajbanshi<sup>1</sup>, S. Roy<sup>2</sup>, Somnath Nag<sup>3</sup>, Abhijit Bisoi<sup>1</sup>, S. Saha<sup>2</sup>, J. Sethi<sup>2</sup>, T. Trivedi<sup>4</sup>,  
T. Bhattacharjee<sup>5</sup>, S. Bhattacharyya<sup>5</sup>, S. Chattopadhyay<sup>1</sup>, G. Gangopadhyay<sup>6</sup>, G.  
Mukherjee<sup>5</sup>, R. Palit<sup>2</sup>, R. Raut<sup>7</sup>, M. Saha Sarkar<sup>1</sup>, A. K. Singh<sup>3</sup>, and A. Goswami<sup>1\*</sup>

<sup>1</sup>*Saha Institute of Nuclear Physics, Kolkata 700064, India*

<sup>2</sup>*Tata Institute of Fundamental Research, Mumbai 400005, India*

<sup>3</sup>*Indian Institute of Technology, Kharagpur 721302, India*

<sup>4</sup>*Guru Ghasidas Vishayavidyalaya, Bilaspur 495009, India*

<sup>5</sup>*Variable Energy Cyclotron Center, Kolkata 700064, India*

<sup>6</sup>*University of Calcutta, Kolkata 700009, India and*

<sup>7</sup>*UGC-DAE consortium for scientific Research, Kolkata 700098, India*

(Dated: May 25, 2015)

Lifetimes of the states in the quadrupole structure in  $^{143}\text{Eu}$  have been measured using the Doppler shift attenuation method as well as parity of the states in the sequence has been firmly identified from polarization measurement using the Indian National Gamma Array. The decreasing trends of the deduced quadrupole transition strength  $B(E2)$  with spin, along with increasing  $J^{(2)}/B(E2)$  values before band crossing, conclusively establish the origin of these states as arising out of antimagnetic rotation. The abrupt increase in the  $B(E2)$  values after the band crossing in the quadrupole band, a novel feature observed in the present experiment, may indicates the crossing of different shears configurations resulting in re-opening of shears structure. The results are well reproduced by numerical calculation within the framework of semi-classical geometric model.

PACS numbers: 21.10.Re, 21.10.Tg, 21.60.Ev, 23.20.Lv, 27.60.+j

It is well known that the deviation of a quantal system from spherical symmetry results in the observation of regular band like structure in its excitation spectrum, with the excitation energy proportional to  $I(I+1)$ ,  $I$  being the quantized angular momentum of a state [1]. The deformed nuclei, found in the specific mass regions of the periodic table [2, 3], are the best examples of such quantum rotation. In true sense it is the charge density that deviates from the spherical symmetry which specifies the orientation of the system as a whole. The resulting sequence of rotational levels gives rise to a band structure where the states are connected through strong  $E2$  transitions. The experimental signature of these bands is the observation of almost constant electric quadrupole transition rates which are proportional to the square of the electric quadrupole moment operator [4].

Interestingly, similar regular sequences of the quadrupole transitions have also been observed for nuclei with small quadrupole collectivity, but with different intrinsic properties compared to the strongly deformed systems [5–7]. These type of excitation mechanism was first reported by Zhu *et al.* [8] from the spectroscopic investigation of  $^{100}\text{Pd}$  nucleus. These bands are characterized by decreasing electric quadrupole transition rates  $[B(E2)]$  with increasing spin [9–15]. The intriguing feature of the falling trend of the  $B(E2)$  values of these sequences has been visualized as a new form of quantized rotation, known as antimagnetic rotation

(AMR) that has also been interpreted in the framework of shears mechanism [16]. In this description the angular momentum is generated by closing of the two blades of conjugate shears, produced by the valence particles (holes). These valence particles (holes) are initially aligned in the time reversed orbit at the band head [16]. There is no net perpendicular component of the magnetic dipole moment for this configuration and it is symmetric with respect to rotation by  $\pi$  about the total angular momentum axis (rotational axis). The resulting quadrupole transition strength will decrease with the increase of spin along the band due to the gradual closing of the angular momentum blades.

Another type of regular band-like structure with different characteristic features but same decreasing trend of  $B(E2)$  values was observed for several nuclei in the mass  $A \sim 110$  and 160 regions [17] and has been interpreted as smoothly terminating bands. These bands show the characteristic of gradually decreasing dynamic moments of inertia with increasing spin in contrast to fairly constant dynamic moment of inertia (without any collective contribution) in the case of the antimagnetic rotation [11]. The calculations show that these bands arise when a particular configuration evolves continuously from high collectivity at low spin to a point where all the spin vectors of the valance nucleons, are aligned. With increasing spin the intrinsic shape evolves until it is symmetric around the axis of rotation. Since collective rotation about the symmetry axis is forbidden, no further angular momentum can be generated through collective rotation and thus represents the termination of the rotational band. The difference between this mechanism and

---

\*Electronic address: asimananda.goswami@saha.ac.in

the antimagnetic rotation is reflected in the variation of dynamic moment of inertia [ $J^{(2)}$ ] and  $B(E2)$  strength as a function of spin. In case of smoothly terminating bands the ratio  $J^{(2)}/B(E2)$  remain almost constant in contrast to sharp increase in the case of the antimagnetic rotation [11].

The observation of conjugate shear structure responsible for the generation of angular momentum in near spherical systems in the form of AMR is also associated with the possibility of a similar complementary excitation mode called magnetic rotation (MR) due to single shear structure [16]. Indeed different manifestation of the shears mechanism with single shear structure have been found in mass regions viz.  $A \sim 80, 100, 140$  and  $190$  [18–27]. Since both these two types of quantized rotation are the consequence of the shear mechanism, it is expected to observe both of them in the mentioned mass regions. However, till day, simultaneous occurrence of these two phenomena have been observed only in mass  $\sim 100$  region where firm experimental evidence of antimagnetic rotation has been reported in several Cd [9–14] isotopes and in the  $^{104}\text{Pd}$  nucleus [15] along with the observation of MR bands [22, 23]. These bands have been interpreted in the framework of simple geometric model [14, 28, 29] and as well as the fully self-consistent microscopic tilted axis cranking method based on covariant density functional theory [30]. For the mass  $A \sim 140$  region, the observed quadrupole band in  $^{144}\text{Dy}$  [31] has been identified as a possible candidate for antimagnetic rotation on the basis of theoretical arguments. However, due to the absence of lifetime data, the nature of excitation mechanism for this band cannot be firmly establish as antimagnetic rotation.

In the present letter, observation of AMR band is reported for the  $^{143}\text{Eu}$  nucleus. The AMR phenomenon in the present case has been established on the basis of the decreasing  $B(E2)$  values with increasing spin for the band of interest. Further-more, a sudden increase of the  $B(E2)$  value, at a higher spin, followed by a another rapid decrease has been observed. This is the first nucleus to exhibit such a behaviour and novel feature in the context of the AMR band.

The lifetimes of the excited states in  $^{143}\text{Eu}$  have been measured using Doppler shift attenuation method (DSAM). The excited states in the  $^{143}\text{Eu}$  nucleus have been populated through the  $^{116}\text{Cd} (^{31}\text{P}, 4n)$  reaction at a beam energy of 148-MeV. The beam was delivered by the Pelletron Linac Facility at the Tata Institute of Fundamental Research (TIFR), Mumbai. The target was 2.4 mg/cm<sup>2</sup> thick  $^{116}\text{Cd}$ , enriched to 99%, on 14.5 mg/cm<sup>2</sup> Pb backing. Indian National Gamma Array (INGA) [32, 33], consisting of nineteen Compton suppressed clover detectors, was used to detect the de-exciting  $\gamma$  rays. The experimental aspects and data analysis are detailed in Ref. [34].

The earlier studies on  $^{143}\text{Eu}$  [35] reported a quadrupole cascade of  $E2$  transitions, connected to the lower part of the level scheme by a 803.9-keV  $E1$  transition. All the reported transitions [35] have been observed in the

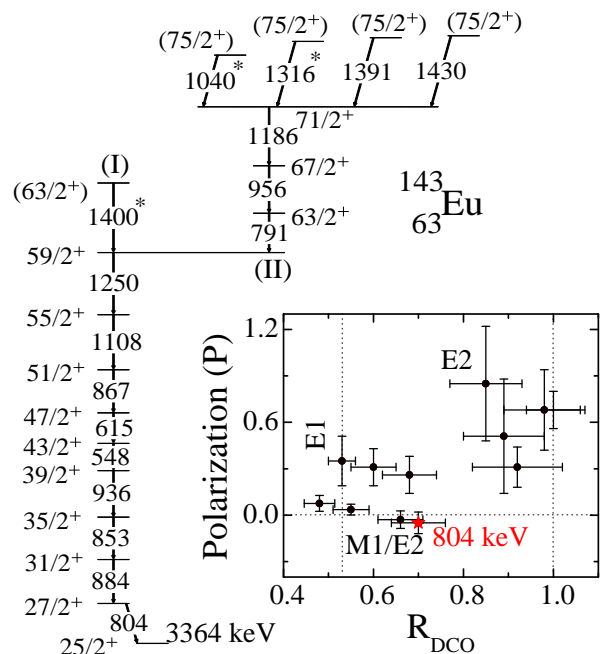


FIG. 1: (Color online) The partial level scheme of the quadrupole structure in  $^{143}\text{Eu}$ . In the inset figure shows the variation of polarization vs DCO ratios (gate on  $E2$  transitions) for different transitions in  $^{143}\text{Eu}$ . The value for the 803.9 keV is represented by the filled red star. The level energy and gamma energies are rounded off to the nearest keV. The new transitions are indicated by an asterisk.

present measurements except for three new transitions which were placed in the partial level scheme [Fig. 1]. The values of DCO ratio, anisotropy and linear polarization determined from the present experiment for the 803.9 keV transition have been found to be 0.70(0.06), 0.78(0.09) and -0.05(0.07), respectively [inset of Fig. 1]. These values conclusively establish that the 803.9 keV transition is of mixed character [with  $M1/E2$  mixing ratio 0.15(0.05)]. Thus the reported  $E2$  cascade has been identified as a positive parity sequence [Fig. 1]. In addition to the previously observed transitions, a weak 1400.0-keV transition parallel to 790.9-keV  $\gamma$  ray is observed above the 1249.7-keV transition. We have also observed two more weak transitions of energies 1316.0 and 1040.0 keV feeding the 71/2+ state. Fig. 2 shows the alignment plot for the quadrupole structure in  $^{143}\text{Eu}$  which is indicative of a band crossing at a spin of 59/2+.

The Doppler-broadened line shapes have been observed for the transitions above the  $I^\pi = 43/2^+$  state in  $^{143}\text{Eu}$ . The level lifetimes of the states have been extracted by fitting these line shapes using the LINESHAPE analysis code [37, 38]. The slowing down history of 10,000 recoil nuclei, traversing the target and the backing media, have been simulated by Monte Carlo techniques with a time step of 1.5 fs. The Shell corrected stopping powers of Northcliffe and Schilling [39] have been used for

TABLE I: Measured level lifetimes ( $\tau$ ) and the corresponding  $B(E2)$  values for the quadrupole transitions in  $^{143}\text{Eu}$ . Dynamic moment of inertia  $J^{(2)}$  and the ratio of  $J^{(2)}/B(E2)$  are also shown for the same transitions.

Sequence	$I_i^\pi$ [ $\hbar$ ]	$E_\gamma$ [keV]	$\tau^a$ [ps]	$\tau^b$ [ps]	$B(E2)$ [ $e^2b^2$ ]	$J^{(2)}$ [ $\hbar^2\text{MeV}^{-1}$ ]	$J^{(2)}/B(E2)$ [ $\hbar^2\text{MeV}^{-1}/(eb)^2$ ]
Structure I	47/2 <sup>+</sup>	614.8	3.1(3)	$2.76^{+0.42}_{-0.35}$	$0.34^{+0.05}_{-0.04}$	15.9	$47^{+8}_{-7}$
	51/2 <sup>+</sup>	866.5	0.6(2)	$0.66^{+0.14}_{-0.10}$	$0.25^{+0.05}_{-0.04}$	16.6	$66^{+13}_{-11}$
	55/2 <sup>+</sup>	1107.5	< 0.5	$0.37^{+0.08}_{-0.06}$	$0.13^{+0.03}_{-0.02}$	28.1	$216^{+50}_{-33}$
	59/2 <sup>+</sup>	1249.7	< 0.5	$0.44^{+0.06}_{-0.05}$	$0.06^{+0.01}_{-0.01}$	26.6	$444^{+74}_{-74}$
Structure II	63/2 <sup>+</sup>	790.9	< 0.5	$0.48^{+0.08}_{-0.07}$	$0.35^{+0.06d}_{-0.05}$	24.3	$69^{+12}_{-10}$
	67/2 <sup>+</sup>	955.6	0.22(5)	$0.44^{+0.07}_{-0.05}$	$0.23^{+0.04}_{-0.03}$	17.4	$76^{+13}_{-10}$
	71/2 <sup>+</sup>	1185.7	< 0.3	0.38 <sup>c</sup>	0.09 <sup>↑</sup>	19.5	216 <sup>↓</sup>

<sup>a</sup>The level lifetimes are adopted from ref [35].

<sup>b</sup>Present measurements.

<sup>c</sup>Upper limit of level lifetime ( $\tau$ ).

<sup>d</sup>The 65% branching ratio for the 790.9 keV transition [35].

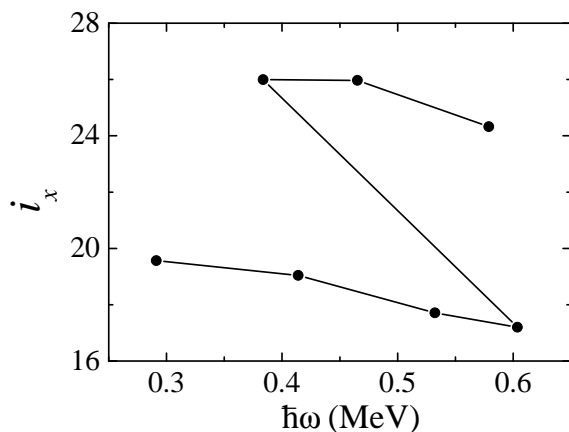


FIG. 2: Experimental aligned angular momentum ( $i_x$ ) for the quadrupole structure (above 43/2<sup>+</sup>) in  $^{143}\text{Eu}$ . The reference parameters were assumed to be  $J_0 = 12 \hbar^2\text{MeV}^{-1}$  and  $J_1 = 25 \hbar^4\text{MeV}^{-3}$ , adopted from ref. [36].

these calculations. These histories have been used to generate angle dependent velocity profiles for detectors at different angles wherein the clover geometry of the detector has been used as an input. The velocity profiles have been used to calculate Doppler shapes for the  $\gamma$ -ray transitions of interest. The experimental spectra have been constructed with gates on the  $\gamma$ -ray transitions below the band of interest. The lifetimes for the states in the band have been extracted by least square fitting of the calculated shapes to the experimental (gated) spectra. The gate on the transitions below the transitions of interest necessitates to consider the side-feeding contribution. This has been modeled with a cascade of five transitions and having a moment of inertia same as that of the band under consideration. Initially, starting from the topmost transition, the members of the band have been sequentially fitted. A direct feeding has been as-

sumed to calculate the shape for the transition from topmost level ( $I^\pi = 71/2^+$ ) for which a clear line shape has been observed. This gives us the value of the effective lifetime of the state. For the subsequent transitions in the band, the transition quadrupole moment, the side-feeding quadrupole moment, the peak height and the background have been used as the free parameters for the least square procedure. Following a satisfactory fit, the spectrum parameters like the peak height and the background have been fixed at the corresponding values. After having fitted all the transitions of the band, sequentially, a global least square minimization has been carried out for all the transitions of the cascade, simultaneously, wherein only the transition quadrupole moment and the side-feeding quadrupole moments for each state have been kept as free parameters.

In the present work, the observed line shapes at angles 65°, 90° and 140° have been fitted simultaneously to obtain the level lifetimes recorded in Table I along with the derived  $B(E2)$  values. The representative line shape fits are illustrated in Fig. 3. The uncertainties in the lifetimes have been derived from the behavior of the  $\chi^2$  fit in the vicinity of the minimum. The quoted errors in the lifetimes do not include the systematic error due to the uncertainty in the stopping power which can be as large as 15%. The level lifetimes have been evaluated in the present analysis by considering the side feeding from both observed as well as unobserved transitions to the level under consideration [23]. Thus the lifetime for the 47/2<sup>+</sup> state has been evaluated by including the 969 keV transition [35] in the feeding history parallel to the 866.5 keV transition. The 969 keV transition appears to be a fully stopped peak in the present experiment. For the next higher lying state at 51/2<sup>+</sup>, it was observed that the state was populated by a 698 keV transition (53/2<sup>+</sup> → 51/2<sup>+</sup>; not shown in Fig. 1) in addition to the 1107.5 keV transition also. We have observed line shapes for both these transitions in the experimental spectra. The partial lifetime for the 51/2<sup>+</sup> state due to the feeding

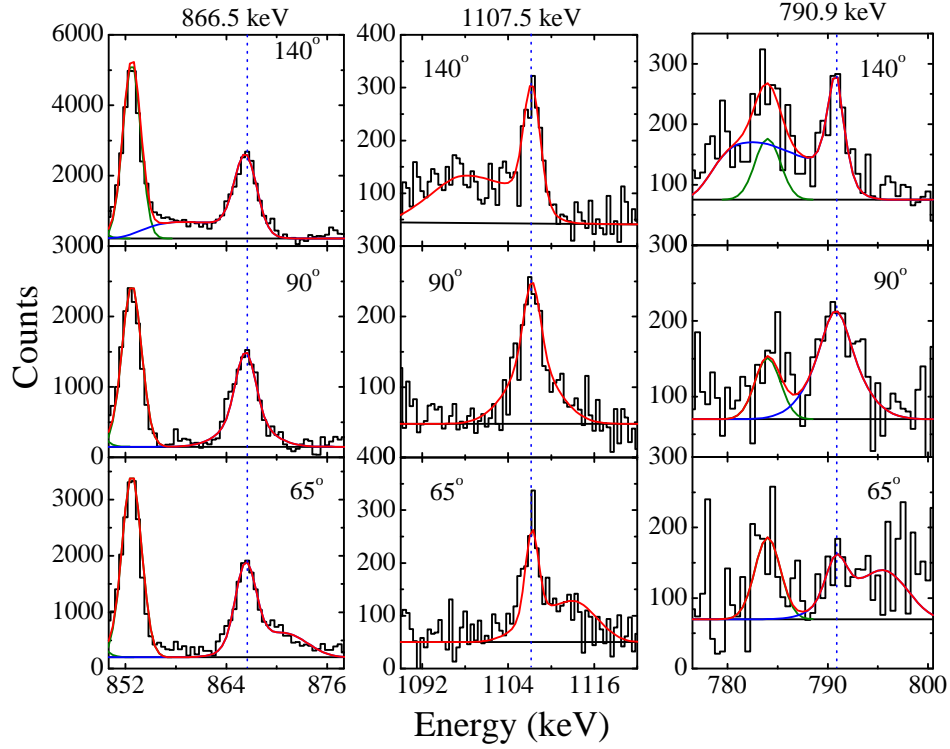


FIG. 3: (Color online) The representative spectra along with theoretically fitted line-shapes for the quadrupole transitions 866.5, 1107.5 and 790.9 keV of quadrupole structure in  $^{143}\text{Eu}$ . Calculated line-shape of  $\gamma$  transitions, contaminant peaks and total line-shapes are represented by the blue, olive and red curves, respectively.

of 698 keV transition has been evaluated. In the final analysis, the top feed lifetime for the  $51/2^+$  level was assumed to be the intensity weighted average of the lifetimes for  $55/2^+$  and  $53/2$  levels since this level was fed by both 1108 keV ( $55/2^+ \rightarrow 51/2^+$ ) and 698 keV ( $53/2 \rightarrow 51/2^+$ )  $\gamma$  rays [40]. The side feeding intensity in all the levels was fixed to reproduce the observed intensity pattern at  $90^\circ$  with respect to the beam direction. The present analysis is validated by the close compliance of the lifetimes of  $47/2^+$  and  $51/2^+$  states, measured in the present work, with those reported in Ref. [35]. For the states above the  $51/2^+$  level, Ref. [35] only provided an upper limit on the lifetimes except for the  $67/2^+$  level.

The Figure 4 (a) shows the variation of the deduced  $B(E2)$  values with spin for the observed quadrupole band in  $^{143}\text{Eu}$ . The  $B(E2)$  value shows a rapid decrease up to the state with spin-parity  $59/2^+$  (marked as (I) in Fig. 4 (a)). For the next higher lying state at  $63/2^+$  it shows a sudden increase and again continues to decrease along the band (marked as (II) in Fig. 4 (a)). The rapid increase of  $J^{(2)}/B(E2)$  ratios with increasing spins (Table I) before band crossing clearly exclude the possibility of the structure I having a smoothly terminating origin. The trend of the  $B(E2)$  values and  $J^{(2)}/B(E2)$  ratios are the definitive experimental signature for the AMR phenomenon so far as structure I is concerned. This is the conclusive experimental evidence of the AMR band observed in any

mass region other than  $A \sim 100$ . The behaviour of the structure II will be discussed later.

The  $^{143}\text{Eu}$  ( $Z = 63, N = 80$ ) nucleus has one proton hole and two neutron holes with respect to the semi-magic nucleus  $^{146}\text{Gd}$ . However protons can be easily excited to the  $h_{11/2}$  orbital across  $Z = 64$  subshell closure, leading to the observation of the magnetic rotational bands. Such bands have been observed in the neighboring  $^{142}\text{Sm}$ ,  $^{141}\text{Eu}$ ,  $^{142}\text{Gd}$  nuclei, which were interpreted in the framework of the tilted axis cranking and the shears mechanism with the principal axis cranking model using small oblate deformation [34, 41, 42].

In contrast to the previous work [35], we have assigned the configuration  $(\nu h_{11/2}^{-2} \pi(d_{5/2}/g_{7/2})^{-3})_{37/2} \otimes (\pi h_{11/2}^2)_0$  to the  $43/2^+$  state (previous assignment was  $\pi(d_{5/2}^{-1}g_{7/2}^{-1}h_{11/2}) \nu h_{11/2}^{-2}$ ). This is due to the fact that for oblate deformation, three proton holes in the  $d_{5/2}/g_{7/2}$  orbitals, being rotation aligned, along with two neutron holes in the  $h_{11/2}$ , produce a total angular momentum of  $37/2^+$ . This is close to the band head spin of  $43/2^+$  for the proposed antimagnetic rotational band (structure I). The difference ( $3\hbar$ ) can be attributed to the contribution of the core. On the other hand, the two protons in the time reversed  $h_{11/2}$  orbital produce two angular momentum vectors which are anti-aligned to each other and perpendicular to the total angular momentum of the



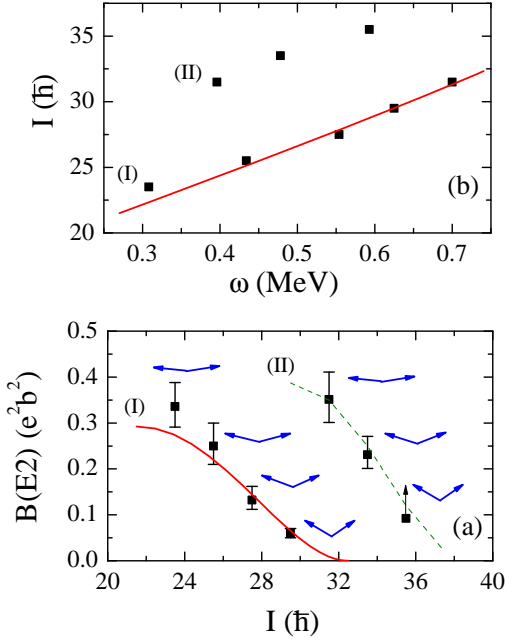


FIG. 4: (Color online) Experimental (a)  $B(E2)$  values with spin  $[I(\hbar)]$  and (b)  $I(\hbar)$  against rotational frequency ( $\omega$ ) for quadrupole band in  $^{143}\text{Eu}$ . The solid red line represents the theoretical semi-classical particle plus rotor model calculation. The parameters used for this calculation are  $V_{\pi\nu} = 1.7\text{-MeV}$ ,  $V_{\pi\pi} = 0.2\text{-MeV}$ ,  $j = 11/2$ ,  $n = 10$ ,  $a = 3.91$  and  $eQ_{eff} = 1.40$  eb. The parameters have same meaning as in Ref. [14, 29]. The arrows depict the relative orientation of the  $h_{11/2}$  proton blades for structure I and structure II. Theoretical  $B(E2)$  values, represented by olive dash line ( $j_h = 59/2\hbar$ ,  $j_\pi = 9/2\hbar$  and  $eQ_{eff} = 1.58$  eb), are calculated using Eq. (1) for structure II.

rotation aligned holes. Thus, for this configuration the double shear structure can exist. We have calculated the band head energy for the above configuration using a particle hole calculation in the relativistic mean field approach [43] using the blocked BCS method. The calculated energy of the band head is found to be 6.8 MeV whereas the corresponding observed value is 7.4 MeV. The difference may be due to the effect of core rotation which is not considered in the present relativistic mean field calculations. It has also been observed from the calculations that the potential energy surfaces for the seven quasi-particle state is much deeper ( $\sim 700$  keV) for oblate deformation compared to prolate deformation.

In order to explore the possibility of the antimagnetic rotational band in  $^{143}\text{Eu}$  for the above mentioned configuration, we have performed a numerical calculation within the framework of a self-consistent semi-classical rotor plus shears model [14, 29] based on the proton-neutron residual interaction [44]. In this model the total energy of an excited state is the sum of the rotational energy of the weakly deformed core and the effective inter-

action energy between the shears blades. The transition probability of the state in the antimagnetic shear can be expressed as [14, 29],

$$B(E2) = \frac{15}{32\pi} (eQ_{eff})^2 \sin^4\theta \quad (1)$$

where  $\theta$  is the angle between the rotational axis and any one of the proton angular momentum vectors.

Experimental  $I(\omega)$  values have been compared with the calculations from the semi-classical rotor plus shears model in Fig. 4(b). The good agreement seems to indicate that the structure I originates due to the antimagnetic rotation with the configuration  $\nu h_{11/2}^{-2} \pi(d_{5/2}/g_{7/2})^{-3} \otimes \pi h_{11/2}^2$ . In order to validate this proposition, the  $B(E2)$  values have been computed using Eq. (1) where the shears angle for each angular momentum state has been calculated from the semi-classical model. These values are represented by the solid line in Fig. 4(a). This agreement provides the essential self-consistency check. The presence of the 1400.0-keV transition above the  $59/2^+$  state may indicate the termination of the aforesaid band at a spin of  $63/2^+$  state due to the complete alignment of two  $h_{11/2}$  protons leading to an angular momentum gain of  $10\hbar$ . Thus, the present calculations seems to indicate that the sequence I originates due to the AMR in a oblate nucleus. This is a unique observation since all the nuclei of the  $A \sim 100$  are prolate where the AMR has been established.

It has been observed from Fig. 4 (a) that there is a large increase of  $B(E2)$  value at a spin of  $63/2^+$ . This nature of variation in the  $B(E2)$  value, an unique feature of the current observation, has not observed in any nucleus. However, such sudden increase in  $B(M1)$  values observed in different mass regions and have been interpreted as a crossing of the two magnetic rotational bands [19, 45, 46]. Thus, the observation may be associated to the emergence of a new double shear structure. This possibility is also supported by the fact that the original AMR structure can generate spin only upto  $63/2^+$  and the observed states with higher angular momentum must have a different single particle configuration, resulting in a re-opening of the shear structure. A new configuration  $[\nu h_{11/2}^{-2} \pi(d_{5/2}/g_{7/2})^{-3} \pi h_{11/2}^2 + \text{core}(3\hbar)]_{59/2} \otimes \pi h_{11/2}^2$  has been tentatively assigned for the quadrupole structure II where two additional  $h_{11/2}$  protons in the time reversed orbit start to align. This is in addition to the rotation aligned spin ( $59/2$ ) due to the structure I. The coupling of these angular momentum vectors may be visualize as another twin shear like structure responsible for the generation of a different AMR band with a new shear angle.

The semi-classical model calculation agreed well with the experimental  $B(E2)$  values for the structure II (Fig. 4(a)) assuming the fact that the proton blades are not fully stretched. Such non-stretched configurations have been assumed in semi-classical calculation [34, 41, 42] in this mass region. In this calculation, the values of

shears angle ( $\theta$ ) are obtained directly from the relation  $I = j_h + 2j_\pi \cos\theta$  for the assumed configuration where  $j_h$  is the total angular momentum of the quasi particles aligned along the rotational axis at the band head and the angular momentum assumed due to the rotation of the core. In this case the maximum spin that can be generated due to the alignment of two more protons in  $h_{11/2}$  is  $6\hbar$  because of Pauli blocking (as two protons are already aligned corresponding to the projection  $11/2$  and  $9/2$  for the sequence I, the available projected states for the next pair of  $h_{11/2}$  protons are  $7/2$  and  $5/2$ ) and hence, this band is expected to generate a maximum spin of  $71/2^+$  which corroborated with the experimental results. The presence of high energy transitions above the state at  $71/2^+$  may visualize as the termination of the AMR band. However, the increasing trend of the  $J^{(2)}/B(E2)$  ratios for the structure II [Table I] can not be definitely ascertain from the present experimental data. Hence the possibility of smooth band termination for structure II cannot be excluded [17].

In summary, the high spin quadrupole structure in  $^{143}\text{Eu}$  has been investigated using the reaction  $^{116}\text{Cd}$  ( $^{31}\text{P}$ ,  $4n$ ) at a beam energy of 148-MeV. Lifetimes of the levels in the quadrupole structure have been measured. The deduced  $B(E2)$  values decrease with increasing spin (and also increase of  $J^{(2)}/B(E2)$  values), indicating the band (structure I) to be of AMR origin, followed by a sudden increase at spin-parity  $63/2^+$ . The configuration  $\nu h_{11/2}^{-2} \pi(d_{5/2}/g_{7/2})^{-3} \otimes \pi h_{11/2}^2$  has been assigned to the structure I from the semi-classical model calculation, which clearly shows that the quadrupole band (structure I) in  $^{143}\text{Eu}$  originate due to the antimagnetic rotation. For structure II a tentative configuration of  $[\nu h_{11/2}^{-2} \pi(d_{5/2}/g_{7/2})^{-3} \pi h_{11/2}^2 + \text{core}(3\hbar)]_{59/2} \otimes \pi h_{11/2}^2$  has been assigned. The  $B(E2)$  values for the states in

quadrupole structure II have been well reproduced within the framework of semi-classical shears model from which it may be concluded that this band may also be originated due to AMR, but the possibility of smooth band termination can not be ruled out. The sudden rise of the  $B(E2)$  value at  $63/2^+$  may be due to crossing of the two antimagnetic rotational band. However such band crossing phenomenon is not incorporated in the present semi-classical model [14, 29]. Detailed investigation in the framework of microscopic model may lead to a better understanding of this behavior. The present measurements conclusively establish the antimagnetic rotation in  $A \sim 140$  region. This observation outside the  $A \sim 100$  region establishes the antimagnetic rotation phenomenon as an alternative mechanism for generation of high angular momentum states in weakly deformed nuclei.

### Acknowledgements

The authors gratefully acknowledge the financial support by the Department of Science & Technology (DST) for INGA project (No. IR/S2/PF-03/ 2003-II). We would like to acknowledge the help from all INGA collaborators. We are thankful to the Pelletron staff for giving us steady and uninterrupted  $^{31}\text{P}$  beam. S. R would like to acknowledge the financial assistance from the Council of Scientific & Industrial Research (CSIR), Government of India under Contract No. 09/489(0083)/2010-EMR-1. A. B (Contract No. 09/489(0068)/2009-EMR-1) and S. N (Contract No. 09/081(0704)/2009-EMR-I) also would like to acknowledge CSIR for financial support. G. G acknowledges the support provided by the University Grants Commission, Departmental Research Support (UGC-DRS) Program.

- 
- [1] A. Bohr and B. R. Mottelson, Phys. Rev. **90**, 717 (1953).
  - [2] S. Raman, C. W. Nestor, Jr, P. Tikkanen, At. Data Nucl. Data Tables **78**, 1 (2001).
  - [3] N. J. Stone, At. Data Nucl. Data Tables **90**, 75 (2005).
  - [4] A. Bohr and B. R. Mottelson, Nuclear Structure Vol. II (Benjamin, 1975).
  - [5] C. J. Chiara *et al.*, Phys. Rev. C **61**, 034318 (2000).
  - [6] M. Sugawara *et al.*, Phys. Rev. C **86**, 034326 (2012).
  - [7] P. H. Regan *et al.*, Nucl. Phys. **A 586**, 351 - 376 (1995).
  - [8] S. Zhu *et al.*, Phys. Rev. C **64**, 041302(R) (2001).
  - [9] A. J. Simons *et al.*, Phys. Rev. Lett. **91**, 162501 (2003).
  - [10] P. Datta *et al.*, Phys. Rev. C **71**, 041305(R) (2005).
  - [11] A. J. Simons *et al.*, Phys. Rev. C **72**, 024318 (2005).
  - [12] Deepika Choudhury *et al.*, Phys. Rev. C **82**, 061308(R) (2010).
  - [13] Deepika Choudhury *et al.*, Phys. Rev. C **87**, 034304 (2013).
  - [14] Santosh Roy *et al.*, Phys. Lett. B **694**, 322 (2011).
  - [15] N. Rather *et al.*, Phys. Rev. C **89**, 061303(R) (2014).
  - [16] S. Frauendorf, Rev. Mod. Phys. **73**, 463 (2001).
  - [17] A. V. Afanasjev *et al.*, Phys. Rep. **322**, 1 (1999).
  - [18] G. Baldsiefen *et al.*, Z. Phys. A **355**, 337 - 338 (1996).
  - [19] Priyanka Agarwal *et al.*, Phys. Rev. C **76**, 024321 (2007).
  - [20] S. Lakshmi *et al.*, Phys. Rev. C **69**, 014319 (2004).
  - [21] D. G. Jenkins *et al.*, Phys. Rev. C **58**, 2703 (1998).
  - [22] N. S. Kelsall *et al.*, Phys. Rev. C **61**, 011301(R) (1999).
  - [23] P. Datta *et al.*, Phys. Rev. C **69**, 044317 (2004).
  - [24] R. Schwengner *et al.*, Phys. Rev. C **65**, 044326 (2002).
  - [25] R. Schwengner *et al.*, Phys. Rev. C **80**, 044305 (2009).
  - [26] Amita, A. K. Jain, and B. Singh, At. Data Nucl. Data Tables **74**, 283 (2000).
  - [27] H. Hübel, Prog. Part. Nucl. Phys. **54**, 1 (2005).
  - [28] R. M. Clark and A. O. Macchiavelli, Annu. Rev. Nucl. Part. Sci. **50** 1 (2000).
  - [29] S. Roy and S. Chattopadhyay, Phys. Rev. C **83**, 024305 (2011).
  - [30] P. W. Zhao, J. Peng, H. Z. Liang, P. Ring, and J. Meng, Phys. Rev. Lett. **107**, 122501 (2011).
  - [31] M. Sugawara *et al.*, Phys. Rev. C **79**, 064321 (2009).
  - [32] R. Palit *et al.*, Nucl. Instrum. Methods **A 680**, 90 (2012).
  - [33] R. Palit *et al.*, J. Phys. Conf. Proc **420**, 012159 (2013).
  - [34] S. Rajbanshi *et al.*, Phys. Rev. C **89**, 014315 (2014).

- [35] M. Piiparinen *et al.*, Nucl. Phys. **A 605**, 191 - 268 (1996).
- [36] D. M. Cullen *et al.*, Phys. Rev. C **66**, 034308 (2002).
- [37] J.C. Wells, N.R. Johnson, LINESHAPE: A Computer Program for Doppler Broadened Lineshape Analysis, Report No. ORNL-6689, 44 (1991).
- [38] N.R. Johnson *et al.*, Phys. Rev. C **55** (1997) 652.
- [39] L. C. Northcliffe and R.F. Schilling, At. Data Nucl. Data Tables **A 7**, 233 (1970).
- [40] N. Rather *et al.*, Phys. Rev. Lett. **112**, 202503 (2014).
- [41] E. O. Podsvirova, *et al.*, Eur. Phys. J. **A 21**, 1 - 6 (2004).
- [42] A. A. Pasternak, *et al.*, Eur. Phys. J. **A 23**, 191 - 196 (2005).
- [43] R. Raut *et al.*, Phys. Rev. C **73**, 044305 (2006).
- [44] A. O. Macchiavelli *et al.*, Phys. Rev. C **57**, R1073(R) (1998).
- [45] R. M. Clark *et al.*, Phys. Rev. Lett. **78**, 1868 (1997).
- [46] Santosh Roy *et al.*, Phys. Rev. C **81**, 054311 (2010).